Functional hyper-crosslinked resins with tailored adsorption properties for environmental applications

Rachele Castaldo[a], Veronica Ambrogi[b], Roberto Avolio[a], Mariacristina Cocca[a], Gennaro Gentile[a,*], Maria Emanuela Errico[a], Maurizio Avella[a]

[a] Institute for Polymers, Composites and Biomaterials, National Research Council of Italy, Via Campi Flegrei 34, 80078 Pozzuoli, Italy
[b] Department of Chemical, Materials and Production Engineering, University of Naples Federico II, Piazzale Tecchio 80, 80125 Napoli, Italy

*Corresponding author. E-mail address: gennaro.gentile@cnr.it

Abstract. The polar functionalization of vinylbenzyl chloride hyper-crosslinked (HCL) resins with ethanolamine at variable functionalization extent is reported. The functionalization reaction was investigated by a multitechnique approach to confirm the reaction mechanism and to calculate the yield of functionalization. Increasing the amount of ethanolamine inserted onto the HCL resin, the total pore volume of the resins decreased, while the microporous fraction increased and the pore size distribution evolved from bimodal to unimodal. The effect of the functionalization on the adsorption properties of the resins was investigated for CO_2 sequestration and water purification applications, demonstrating that both CO_2 adsorption capacity and phenol removal efficiency from water solutions over the total pore volume of the resins significantly increased. Moreover, the CO_2/N_2 selectivity significantly increased for the HCL resin at intermediate functionalization degree, which represents the optimal trade-off between high functionalization extent and porosity distribution evolution.

Keywords: hyper-crosslinked resins; ethanolamine functionalization; CO_2 selectivity; phenol adsorption; specific surface area; pore size distribution.

Revised Manuscript.

The final version is available at:

https://www.sciencedirect.com/science/article/pii/S1385894719300622

https://doi.org/10.1016/j.cej.2019.01.054

1. Introduction

Due to their outstanding properties, microporous organic polymers (MOPs), characterized by high specific surface area (SSA), are widely applied in several fields, such as purification processes [1,2] gas adsorption and separation [3,4,5], energy storage [6], molecular separation [7,8] and catalysis [9]. Within MOPs, hyper-crosslinked (HCL) resins represent a very remarkable subclass of materials, whose scientific interest has recently increased due to the development of new versatile synthetic strategies able to simplify their production and to enlarge their applications [5,10,11], using for instance HCL materials as functional fillers in polymer matrices for water remediation [12]. HCL resins also stand out for the possibility of tuning their properties by a wide range of effective approaches [13], such as modulating their porosity and pore size distribution by properly designing the polymer structure [14,15,16], or by tuning their polarity and adsorption capacity by embedding functional nanostructured fillers [17] or by inserting functional groups [18,19].

In particular, nitrogen enriching of porous carbon materials is one of the most investigated strategies to realize materials able to selectively adsorb CO_2 for environmental applications [20,21]. Indeed, CO_2 adsorption was successfully improved by the design and development of suitable porous adsorbent supports onto which amine-containing groups were attached or immobilized. This type of materials are often called solid amine sorbents. Different approaches were used for the insertion of amines onto HCL resins, including impregnation and direct co-polymerization [22]. For instance, a HCL divinylbenzene resin was impregnated with tetraethylenepentamine (TEPA), demonstrating that optimized TEPA loading provides active sites for CO_2 capture, whereas excessive loading induces TEPA aggregation and blockage of pore channels [23]. An interesting example of direct co-polymerization of amine-containing monomers was also reported, based on the synthesis of porous poly(methacrylamide-co-ethylene glycol dimethacrylate) polymeric particles. In these systems, the presence of the amine-containing methacrylamide monomer induced high CO_2-philicity at low pressures [24].

Moreover, interesting studies were focused on the development of polar HCL resins to improve their adsorption capability towards polar aromatic pollutants for water remediation applications. In particular, vinylbenzyl chloride (VBC) based resins modified with ethylene glycol dimethacrylate (EGDMA) were synthesized, showing improved adsorption capacity toward phenol, p-nitrophenol, and Rhodamine B as a function of the EGDMA functionalization extent [25]. With a different approach, N-vinylimidazole was co-polymerized with VBC for the realization of HCL resins. By optimization of the feeding amount of N-vinylimidazole and VBC monomers, the polarity and pore size distribution of the resins were finely tuned, inducing a selective adsorption of benzoic acid and Rhodamine B from water solutions [26].

Starting from these results, in this work a functionalization strategy based on the grafting of a polar functional molecule, containing both hydroxyl and amino functional groups, onto a high surface area HCL resin is reported. The objective was to simultaneously induce an improvement of the CO_2-philicity and polarity of the resin, for selective gas sorption and water remediation applications. A Davankov-type HCL resins based on VBC and divinylbenzene (DVB) was selected as high SSA support and an alkanolamine, namely ethanolamine (ETA), was selected as functional modification group. The functionalization was performed by alkylation of ETA with chloromethyl groups of the poly(VBC-co-DVB) precursor. The mechanism and the yield of the modification reaction was investigated by Fourier transform infrared (FTIR) spectroscopy, thermogravimetric analysis (TGA) and solid state nuclear magnetic resonance (NMR). The modified resins were characterized by N_2 and CO_2 adsorption tests to evaluate the effect of the ETA functionalization on the porosity and pore size distribution of the HCL resin and on its selective adsorption towards CO_2. Moreover, phenol adsorption tests from water solutions were performed to evaluate the water remediation capability of the polar HCL resins towards polar organic pollutants.

2. Experimental section

2.1. Materials

Vinylbenzyl chloride (VBC, ≥95.0%, mixture of isomers, ∼70% meta + ∼30% para), p-divinylbenzene (DVB, 85%, meta isomer ∼10 wt %), 2,2′-azobis(2-methylpropionitrile) (AIBN, >98%), ethanolamine (ETA, >98%), $FeCl_3$ (≥97%), phenol (>99.5%), and all solvents were purchased by Sigma-Aldrich (Milan, Italy) and used without further purification.

2.2. Preparation of the HCL polymers.

Poly(vinylbenzyl chloride-co-divinylbenzene) (DV) was synthesized through bulk polymerization. DVB and VBC were mixed in a 2:98 molar ratio, 0.5 phr of AIBN were added and the mixture was kept at 80°C in a flask for 30 minutes under nitrogen. Therefore, the mixture was poured in a sealed glass vial and cured in oven for 24 h at 80°C, then purified by multiple washings with methanol, acetone and diethyl ether, and dried in a vacuum oven at 40 °C for 24 h.

Ethanolamine-functionalized DV samples were obtained as follows. The precursor polymer DV was placed in a flask containing DMF (20 mg/mL), and ethanolamine was added. The amounts of ethanolamine were set on the basis of the nominal amount of chloromethyl groups in the DV precursor, i.e. the amount of VBC monomer unit. In details, the following ethanolamine/-CH_2Cl molar ratios were used: 0.15, 0.30 and 0.50. The mixtures were stirred at 60 °C for 4 hours. Then, the resins were washed and dried, as reported for DV. The corresponding samples were coded DV1, DV2 and DV3, respectively.

Plain (DV) and functionalized (DV1, DV2, DV3) resins were hyper-crosslinked by Friedel−Crafts reaction. Precursors were swollen in 1,2-dichloroethane (DCE), under nitrogen flow for 2 h. Then the mixtures were cooled to 0 °C in an ice/water bath, and $FeCl_3$ was added. Therefore, the system was heated to 80 °C and kept at this temperature for 18 h. The hyper-crosslinked resins were washed with methanol and dried under vacuum at 80 °C. Samples were coded as the corresponding precursor resins adding the prefix X (XDV, XDV1, XDV2 and XDV3). DV was also subjected to a much briefer hyper-crosslinking, reducing the 80°C step to 5 minutes, and this HCL resin was coded as XDV-5min.

2.3. Characterization

The precursor resins were characterized by means of FTIR spectroscopy. Spectra were recorded in attenuated total reflectance (ATR) mode with a PerkinElmer Spectrum One FTIR spectrometer equipped with an ATR module, using a resolution of 4 cm^{-1} and 32 scan collections.

TGA was performed on the HCL resins through a Mettler TGA/SDTA851 analyser, in oxidizing atmosphere, at 10 °C/min heating rate, from room temperature to 800 °C, using about 5 mg of material.

Solid-state ^{13}C single pulse (SP) NMR spectra were collected on all HCL resins by means of a Bruker Avance II 400 spectrometer equipped with a 4 mm magic angle spinning (MAS) probe, using a ^{13}C $\pi/2$ pulse width of 3.9 μs, a repetition time of 40 s and high power proton decoupling. HCL powder samples were packed into 4 mm zirconia rotors sealed with Kel-F caps and spun at a spinning speed of 13 kHz. All spectra were referenced to external adamantane (methylene signal at 38.48 ppm downfield of tetramethylsilane (TMS), set at 0.0 ppm). Line fitting of the spectra was performed by means of the GRAMS/AI 8.0 software package [27], using Gaussian lineshapes.

Scanning electron microscopy (SEM) analysis was performed on HCL samples using a FEI Quanta 200 FEG SEM in high vacuum mode at 10-30 kV acceleration voltage using a secondary electron detector. Before observations, the samples were sputter coated with a 15 nm thick Au-Pd layer.

Specific surface area (SSA) and pore size distribution analysis of the HCL resins were performed using a Micromeritics ASAP 2020 analyzer. SSA was determined by nitrogen adsorption measurements at 77 K from the linear part of the BET equation. Nonlocal density functional theory (NLDFT) was applied to the nitrogen adsorption isotherms to evaluate the pore size distribution of the materials. N_2 and CO_2 adsorption analysis were also performed at 298 K up to 1 bar. CO_2/N_2 selectivity was evaluated by the ideal adsorbed solution theory (IAST) and by quantitative analysis of the isotherms curves in their linear part (up to 140 mmHg). Prior to the analysis all samples were

degassed at 120 °C under vacuum ($P < 10^{-5}$ mbar); all the adsorption measurements were performed using high purity gases (>99.999%).

Phenol adsorption tests from water were performed on neat and functionalized HCL resins at 25 °C in the range of phenol concentration from 100 to 1500 mg/L. About 10 mg of HCL resin was introduced into vials containing 10 mL of the phenol solution. The vials were kept at 25 °C until equilibrium was reached. Therefore, the solution was removed from the vial, and the final phenol concentration was measured using a Jasco V570 UV spectrophotometer. A previously recorded calibration curve was used to determine the phenol concentration from absorbance of the peak centered at 270 nm.

3. Results and discussion

Hyper-crosslinked resins at variable ETA functionalization were prepared by a facile synthetic procedure based on the bulk pre-polymerization of the precursor polymer DV [11], the amino-de-halogenation of DV with ETA and the hyper-crosslinking of the product through Friedel-Crafts reaction. The designed scheme of reaction is reported in Figure 1.

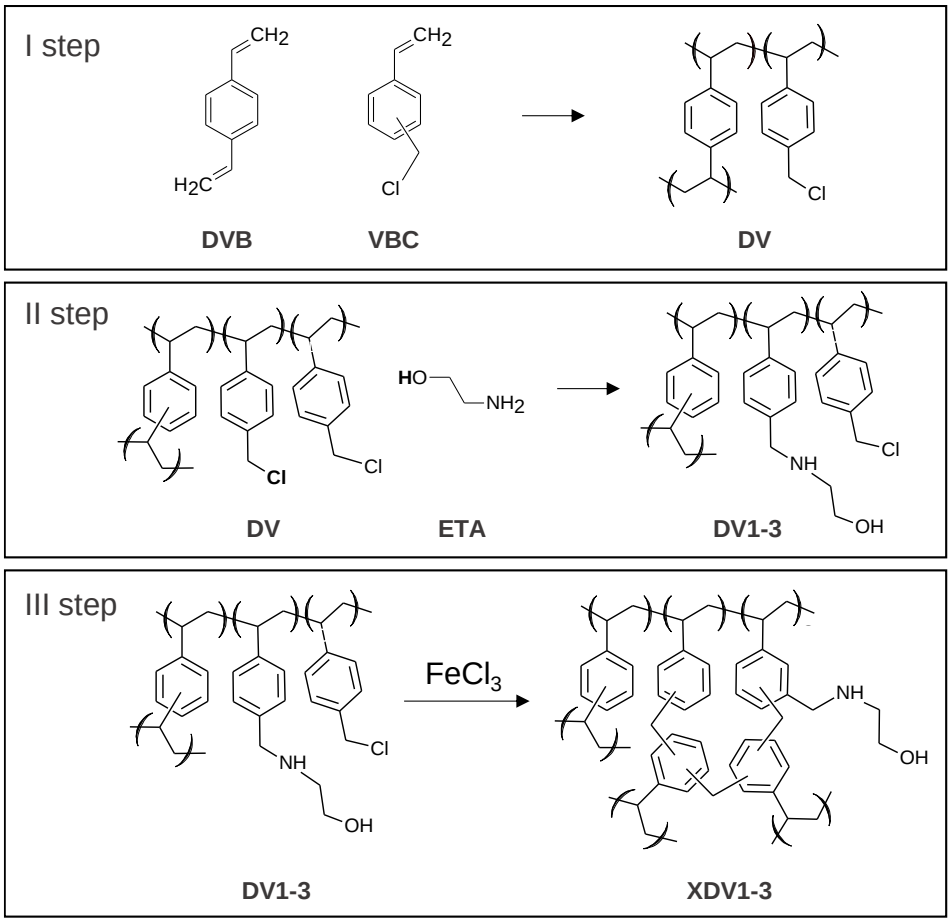

Figure 1. Synthesis of functionalized hyper-crosslinked resins through precursor polymer synthesis (I step), ETA functionalization (II step) and hyper-crosslinking through Friedel-Crafts reaction (III step).

The products DV1-3 obtained by amine-alkylation were analysed by means of FTIR analysis to investigate the extent of functionalization. FTIR spectra, reported in Figure 2a together with the spectrum of the plain precursor DV, show, in the functionalized polymers, a new broad absorption band in the range 3700-3100 cm^{-1}. This signal, attributed to the stretching of -OH and -NH groups, confirms ETA functionalization of DV1-3 precursors. The intensity of this adsorption bands increases with the ETA content, indicating that the functionalization extent can be tailored by varying the amount of ethanolamine. Moreover, DV1-3 precursors show the arising of a new absorption band centred at about 1055 cm^{-1}, attributed to C-O stretching vibrations of ETA. Coherently, a decrease of

the intensity of the characteristic signals of -CH_2Cl wagging vibration mode (1265 cm^{-1}) and C-Cl stretching vibration (670 cm^{-1}) with the insertion of ETA was observed.

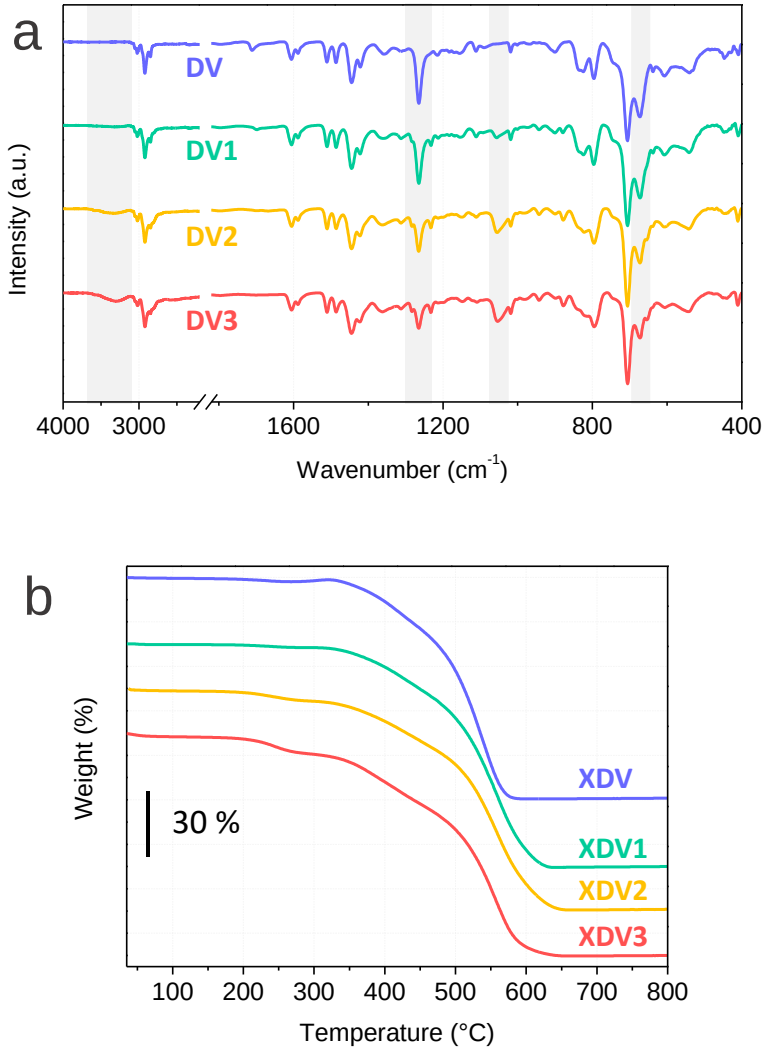

Figure 2. FTIR spectra of plain (DV) and ETA-functionalized (DV1-3) precursor resins (a); TGA curves (b) of plain and functionalized HCL resins.

Thermogravimetric analysis was performed on plain and functionalized HCL resins. Three weight loss steps are evidenced in the thermograms of XDV1-3 (Figure 2b): a first step occurring in the range between 200°C and 300°C, whose extent increases with the ETA functionalization, and two further steps, in the ranges 320°C - 460 °C and 460°C - 600 °C, practically unaffected by the ETA content. On the other hand, plain HCL resin XDV only shows the two degradation steps at higher

temperatures, showing negligible weight loss up to about 320 °C. The degradation of the functionalized HCL resins in the 200°C - 300°C range was attributed to the unzipping of ethanolamine groups. On this basis, from the weight loss at 300 °C (WL_{300}) the amount of ETA groups inserted was estimated as the molar ratio ethanolamine/chloromethyl groups, where the amount of chloromethyl groups are the stoichiometric amount used during the synthesis and before the reaction with ethanolamine (N/VBC). Results are summarized in Table 1. The calculated N/VBC values can be directly compared to the stoichiometric molar ratios used for the ethanolamine functionalization step, i.e. 0.15, 0.30 and 0.50, indicating yields ranging between about 20 and 50%.

Table 1. Quantification of ETA functionalization by TGA and NMR.

sample	**TGA**		**NMR**	
	WL_{300} (%)	N/VBC molar ratio	ETA insertion yield (%)	N/VBC molar ratio
XDV1	1.5	0.03	40	0.06
XDV2	5.7	0.12	47	0.14
XDV3	9.6	0.21	50	0.25

A detailed investigation on the functionalization of the DV precursor resin with ETA was performed by solid state NMR. In particular, this analysis was performed to confirm the hypothesized reaction mechanism as well as to quantify the insertion yield. In Figure 3a, ^{13}C SP NMR spectra of neat (XDV) and modified (XDV1-3) HCL resins are reported. As shown, the spectra of the modified materials display the appearance of a new band in the aliphatic region. This new complex band, centered at ~ 56 ppm, was resolved by line fitting in three peaks, as reported in Figure 3b, corresponding to -$\underline{C}H_2$-OH (~ 60 ppm), and two different -$\underline{C}H_2$-NH, that is, -Ph-$\underline{C}H_2$-NH- (~ 50 ppm) and OH-CH_2-$\underline{C}H_2$-NH- (~ 55 ppm). This assignment allows confirming the ethanolamine insertion mechanism. The reaction involves the amino groups of ethanolamine and the chloromethyl group of the neat resin,

thus resulting in an amine alkylation reaction. The proposed structure of the modified resin is schematized in Figure 1 (II step).

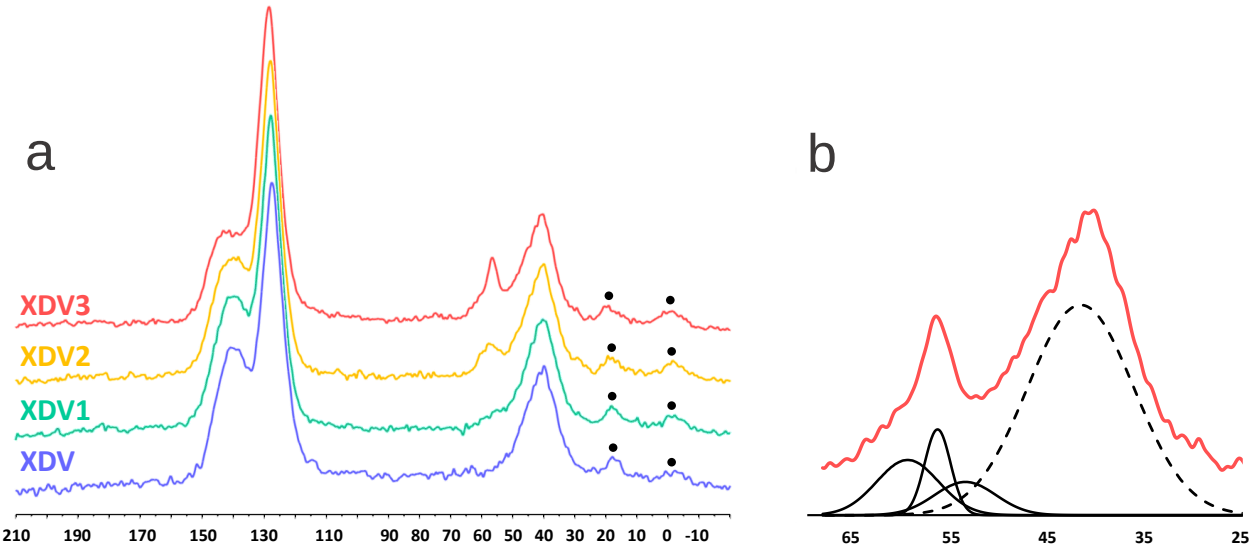

Figure 3. ^{13}C SP NMR spectra of plain and functionalized HCL resins (a, spinning sidebands are marked by a dot). Line fitting of the aliphatic region of XDV3 (b, solid lines: peaks attributed to ethanolamine carbons; dashed lines; backbone carbons).

It is worth to note that also the aromatic region of ^{13}C spectra (110-160 ppm) is affected by the functionalization reaction. A progressive decrease in relative intensity of the low field peak (~ 140 ppm), attributed to sp^2 carbons involved in the hyper-crosslinking reaction, is observed as a function of ETA insertion degree. This finding is correlated to the decreased amount of Cl atoms available for hyper-crosslinking, as also verified by FTIR analysis, thus resulting in a lower crosslinking degree expected for XDV1-3 samples. Finally, the insertion yield was calculated by comparing the intensity of the peaks attributed to the ethanolamine and to the aliphatic carbons of the resin (Table 1). Results are in good agreement with data obtained by TGA, confirming that the weight loss occurring during thermal-oxidation in the range 200-300 °C can be univocally attributed to the ethanolamine unzipping.

The morphology of plain and functionalized HCL resins was analysed by SEM analysis. As previously reported [11], hyper-crosslinking induces extensive fragmentation of the precursor polymers. As a consequence, all HCL samples display irregular particle shape, with dimensions ranging from 10 µm to 150 µm, as shown in Figure 4 for the samples XDV and XDV3, showing that the functionalization of the precursor polymers and the different extent of hyper-crosslinking revealed by solid state NMR for plain and functionalized resins do not significantly affect the final particle dimensions and shape.

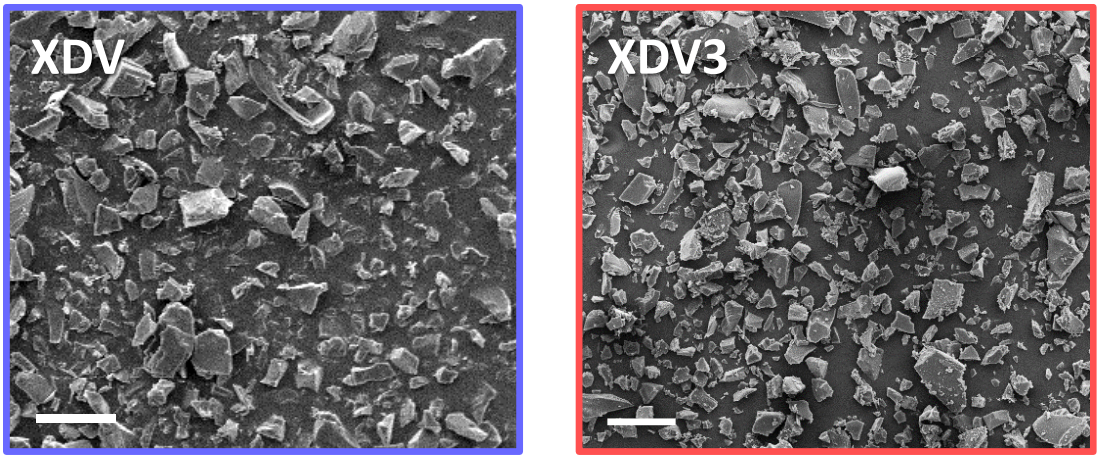

Figure 4. SEM images of HCL resins XDV and XDV3 (scale bars 100 µm).

The effect of ETA functionalization, which involves a reduction of the chloromethyl groups available for crosslinking, on surface area and pore size distribution was investigated by N_2 adsorption at 77 K. As shown in Figure 5a, all samples present a type II isotherm, characterized by very sharp adsorption increase at low pressure and a slower increase at higher pressures. The slope of the N_2 adsorption/desorption curves at high pressure decreases with increasing the degree of functionalization. Moreover, a pronounced hysteresis in desorption is noticeable in XDV isotherm, and its entity decreases with increasing the degree of functionalization in XDV1-3 samples. The sharp increase in the first step of the adsorption isotherm indicates the presence of microporosity, while the increase at higher pressures and the hysteresis loop suggests mesoporosity [28]. Therefore, the shape

of the isotherms suggests a micro/mesoporous distribution in all samples, leaning towards a unimodal distribution with increasing the functionalization degree.

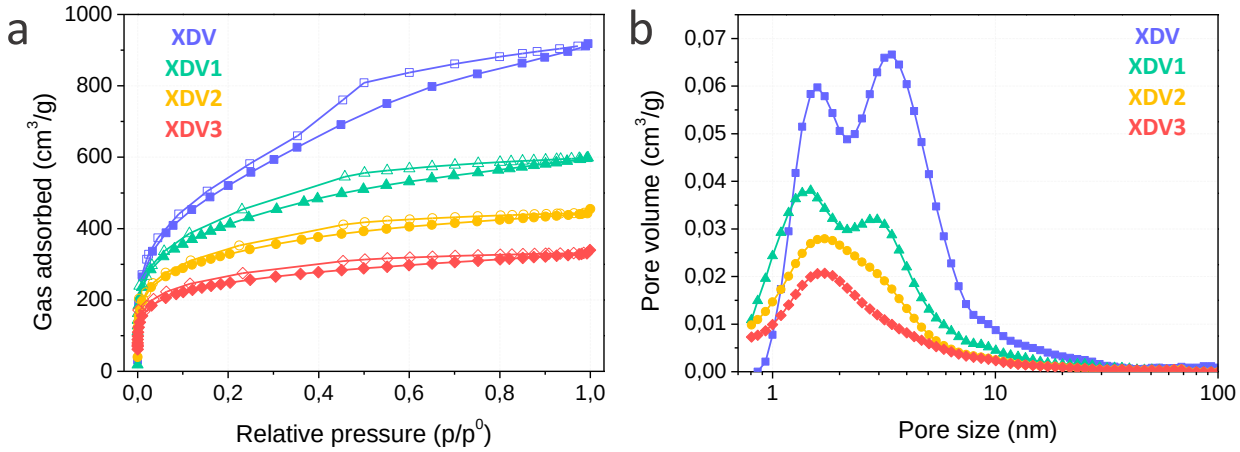

Figure 5. N_2 adsorption and desorption isotherms at 77K of HCL resins (a, adsorption curves in solid points, desorption curves in hollow points); Pore size distribution calculated by NLDFT (b).

This trend is confirmed by NLDFT pore size distribution, shown in Figure 5b. Indeed, XDV is characterized by a bimodal pore size distribution, with major peaks centred at 1.59 nm and 3.43 nm. Increasing the degree of functionalization, the intensity of the peak at higher size progressively decreases. In particular, for XDV2 the mesoporous peak becomes a shoulder of the microporous peak, and the sample shows an interesting hierarchical pore size distribution in the range 0.8 - 5 nm. At the highest functionalization degree, the peak indicative of mesoporosity almost completely disappears in XDV3, which presents a quasi-unimodal distribution centred at 1.72 nm. The quantitative evaluation of the microporosity fraction (MF), i.e. the percent micropores volume over the total pore volume, is summarized in Table 2. As shown, MF increases monotonically with the degree of functionalization, from 32 % in XDV up to 57 % in XDV3.

Table 2. SSA and pore size distribution results, CO_2 uptake and selectivity, Freundlich adsorption parameters.

sample	BET (m^2/g)	pore volume (cm^3/g)	MF (%)	CO_2 uptake* ($mmol/g^1$)	CO_2 uptake* ($mmol/cm^3$)	S_{IAST} **	S_{slope} ***	n	K_F $\left(\frac{mmol/g}{(mmol/L)^1}\right.$	R^2
XDV	1870 ± 20	1.28	32	1.16	0.86	9.6	10.6	1.82	0.55	0.997
XDV1	1400 ± 25	0.81	49	1.15	1.42	8.9	10.4	1.79	0.43	0.995
XDV2	1100 ± 15	0.61	54	1.00	1.63	13.5	15.0	2.10	0.54	0.997
XDV3	870 ± 10	0.46	57	1.02	2.22	9.3	11.9	1.97	0.60	0.998

* calculated at 1 bar and 298 K
** calculated by applying the Ideal Adsorbed Solution Theory
*** calculated by the initial slope of the CO_2 and N_2 adsorption isotherms

This effect can be ascribed to the lower amount of chloromethyl groups available for the Friedel-Crafts hyper-crosslinking, due to their partial removal during functionalization of the precursor polymer with ETA. Indeed, the mechanism of hyper-crosslinking significantly foresees polyalkylation since, once a chloromethyl group reacts with the aromatic ring, the methylene group that bridges two benzene rings activates them to further alkylation. Therefore, Friedel-Crafts alkylation can possibly proceed mainly in regions with high crosslinking degrees, generating clusters of micropores. Moreover, for functionalized samples, due the limited amount of available chloromethyl groups, the reaction is not able to proceed further, extending the hyper-crosslinked network and generating larger pores. This result is comparable to the effect of a brief hyper-crosslinking. To validate this hypothesis, a DV precursor was subjected to a 5-minute hyper-crosslinking in the same conditions employed for XDV and XDV1-3. This sample (XDV-5min) showed a BET SSA of 1380 ± 11 m^2/g, confirming that the most of a HCL polymer interconnected structure and SSA are achieved in the first minutes of the Friedel-Crafts alkylation reaction, as similarly reported by Ahn et al. [29]. Moreover, pore size distribution analysis of XDV-5min revealed a major microporous peak and a minor mesoporous distribution. By comparing this pore size distribution (Figure S1 in Supplementary Information) with the one of XDV, it is highlighted that, in the first phase of the hyper-crosslinking reaction, smaller pores are mostly formed while,

afterwards, bigger pores are generated. The generation of smaller pores is to be attributed to the favourability of the polyalkylation while, once the substitution of the first reacted aromatic rings gets saturated, the bigger pores are formed from the interconnections between adjacent polymeric moieties already connected at the lower scale.

The effects of ETA functionalization and the evolution of pore size distribution on the selective gas adsorption properties of HCL resins were evaluated by measurements of CO_2 and N_2 adsorption at 298 K. On a gravimetric basis, CO_2 adsorption capacity of XDV is 1.16 mmol/g and it remains substantially unchanged passing to XDV1. Instead, a decrease of the CO_2 adsorption capacity is recorded with further functionalization, to about 1.0 mmol/g for both XDV2 and XDV3. This decrease is a direct consequence of the reduced pore volume and the consequent increased specific weight of the functionalized resins. In fact, if considered the specific porosity of the HCL resins, on a volumetric basis, the adsorption of CO_2 increases with functionalization, passing from 0.86 mmol/cm^3 for XDV up to 2.22 mmol/cm^3 for XDV3 (Table 2 and Figure 5a). This increase is mainly attributed to the amino groups of the functionalized resins. Indeed, the presence of amino functionalities enhances CO_2 adsorption due to acid-base interactions between the basic functional amino groups and the acidic CO_2 molecules [30]. Moreover, it is to be remarked that also the presence of -OH functionalities boosts CO_2 adsorption, by hydrogen bonding and dipole-quadrupole interactions [31, 32].

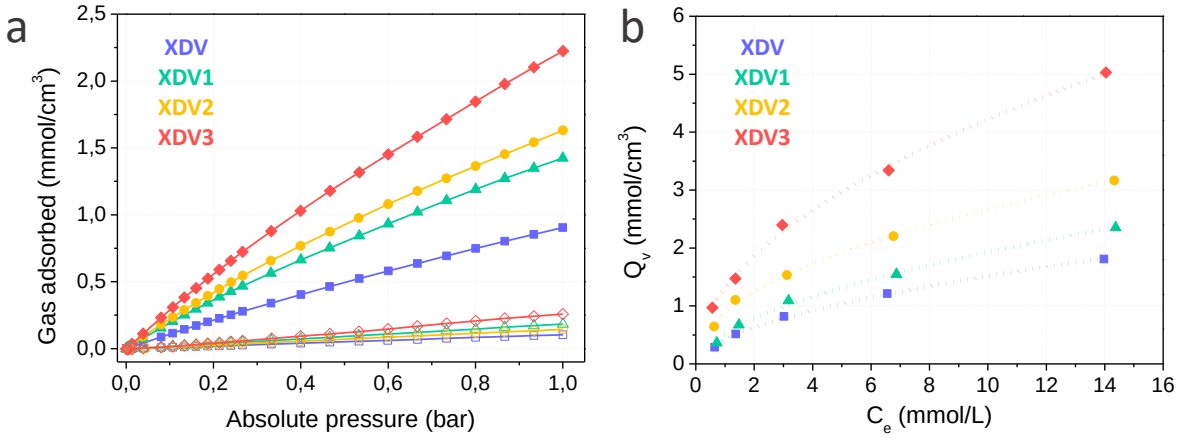

Figure 6. CO_2 (solid points) and N_2 (hollow points) adsorption isotherms (a) and phenol uptake (b, Freundlich fit in dashed curve) at 298 K of plain and functionalized hyper-crosslinked resins.

The selectivity of CO_2 adsorption over N_2 can be calculated from the single-component isotherm data. This kind of evaluation does not consider the competition of gas molecules for the adsorption sites on the pore surface, however it provides a simple way to obtain an evaluation of the performance of different materials in terms of gas sorption selectivity. CO_2 and N_2 adsorption curves at 298 K are reported in Figure 6a. According to the Ideal Adsorbed Solution Theory (IAST), the selectivity of adsorption of CO_2 over N_2 is defined as the ratio of the amount of CO_2 and N_2 adsorbed divided for the corresponding pressures [33]. For CO_2 purification of industrial streams, maximizing low-pressure CO_2 adsorption is highly desirable, since flue gases emitted from coal-fired power stations typically contain CO_2 in quantity of 10 or 15 % [34]. Therefore, the simplest approximation for the composition of flue gas is usually of 15 % CO_2, 75 % N_2 and 10 % other gases, and CO_2/N_2 selectivity S_{IAST} would be expressed as reported in equation (1):

$$S_{IAST} = \frac{(q_{CO_2}/q_{N_2})}{(p_{CO_2}/p_{N_2})} \quad (1)$$

with p_{CO_2} = 0.15 bar and p_{N_2} = 0.75 bar.

As shown in Table 2, amongst XDV and the functionalized resins XDV1-3, an increase of S_{IAST} of about 40 % with respect to XDV was recorded for XDV2. Values of S_{IAST} similar to those recorded

for XDV were found for HCL resins with the lowest (XDV1) and highest (XDV3) functionalization extent. CO_2/N_2 selectivity of plain and functionalized hyper-crosslinked resins calculated following the initial slope comparing method (S_{slope}) confirmed this trend, without significant increase for XDV1 with respect to the plain resin, an increase of S_{slope} of about 50 % for XDV2 and much lower (about 12 %) for XDV3. Therefore, with both methods, CO_2/N_2 gas sorption selectivity is significantly enhanced only for XDV2, i.e. the sample with a high functionalization extent combined to a high microporous and a hierarchical porosity distribution in the range 0.8 - 5 nm. This is well explained considering that selectivity toward CO_2 adsorption is promoted not only by the presence of amino and hydroxyl functional groups, but also by the predominant presence of micropores, due to caging effect, and to a hierarchical porosity [35, 36]. These results suggest that the maximization of the selective adsorption of a material toward CO_2 requires a trade-off between functionalization, total pore volume and pore size distribution.

Phenol adsorption capacity of XDV and functionalized resins from water solutions was evaluated through equilibrium adsorption tests using phenol concentrations in the range 100-1500 mg/L. The recorded data well follow the Freundlich model

$$Q_e = K_F {C_e}^{1/n} \quad (2)$$

where Q_e (mmol/g) is the quantity of phenol adsorbed at equilibrium, C_e is the equilibrium concentration (mmol/L), K_F (mmol/g)(mmol/L)$^{-1/n}$, the Freundlich constant, indicates the adsorption capacity, and n is a parameter suggesting the intensity of the adsorption. Freundlich parameters n and K_F for the plain and functionalized resins and the correlation coefficient of the fitting are reported in Table 2. As shown, despite the relevant progressive reduction of SSA and porosity recorded at increased functionalization extents, both n and K_F, the latter expressed with respect to the weight of the resins, did not significantly change in the functionalized resins. However, it is noteworthy to underline the trend of the phenol adsorption curves per pore volume, shown in Figure 6b. Indeed, in the range of phenol concentration investigated, phenol adsorption per pore volume monotonically increases with the functionalization, reaching at the highest functionalization extent values more than

two-fold higher than plain XDV. In particular, at the highest phenol concentration (1500 mg/L), the equilibrium adsorption capacity increased from 1.8 mmol/cm^3 (XDV) to 2.4, 3.2 and 5.0 mmol/cm^3 for XDV1, XDV2 and XDV3, respectively. This behaviour demonstrate that polar modification of microporous materials represents a promising strategy to design effective materials for water purification from organic pollutants.

4. Conclusions

In this work, a functionalization strategy based on the grafting of ethanolamine (ETA) onto high surface area hyper-crosslinked polymers is reported. HCL polymers based on vinylbenzyl chloride and divinylbenzene at variable ETA functionalization were prepared by amine-alkylation of the precursor polymer followed by hyper-crosslinking through Friedel-Crafts reaction.

The proposed mechanism for the modification reaction was confirmed by FTIR spectroscopy, TGA and solid state NMR. By comparison of the NMR signals attributed to ETA and to resin, a reaction yield up to 50% was calculated.

With increasing the ETA content, BET SSA and total pore volume of the resins decreased, while the microporous fraction increased and the pore size distribution evolved from bimodal to unimodal. In particular, the intermediate composition XDV2 presented hierarchical micro/mesoporosity. Finally, the effect of the functionalization on the adsorption properties of the resins was investigated. Results showed that for ETA functionalized resins, CO_2 and phenol adsorption over total pore volume increased dramatically. In particular, the phenol adsorption capacity at the highest phenol concentration increased from 1.8 (XDV) to 5.0 mmol/cm^3 (XDV3). For what concerns gas sorption, the CO_2 adsorption capacity at 298 K increased from 0.86 (XDV) to 2.22 mmol/cm^3 (XDV3). Moreover, the CO_2/N_2 selectivity significantly increased for the sample at intermediate functionalization degree (XDV2), which showed the optimal trade-off between extent of functionalization and porosity evolution.

References

[1] N. Chaukura, B. B. Mamba, S. B. Mishra, Porous materials for the sorption of emerging organic pollutants from aqueous systems: The case for conjugated microporous polymers, J. Water Process Eng. 16 (2017) 223-232. https://doi.org/10.1016/j.jwpe.2017.02.001.

[2] Yang, R.-X., Wang, T.-T., Deng, W.-Q., 2015. Extraordinary capability for water treatment achieved by a perfluorous conjugated microporous polymer. Sci. Rep. 5, 10155. https://doi.org/10.1038/srep10155.

[3] P. Bernardo, E. Drioli, G. Golemme, Membrane gas separation: a review/state of the art, Ind. Eng. Chem. Res. 48 (2009) 4638-4663. https://doi.org/10.1021/ie8019032.

[4] R. Dawson, A. I. Cooper, D. J. Adams, Nanoporous organic polymer networks, Prog. Polym. Sci. 37 (2012) 530-563. https://doi.org/10.1016/j.progpolymsci.2011.09.002.

[5] H. Gao, L. Ding, H. Bai, L. Li, Microporous organic polymers based on hyper-crosslinked coal tar: preparation and application for gas adsorption, Chem. Sus. Chem. 10 (2017) 618-623. https://doi.org/10.1002/cssc.201601475.

[6] C. Zhang, X. Yang, W. Ren, Y. Wang, F. Su, J.-X. Jiang, Microporous organic polymer-based lithium ion batteries with improved rate performance and energy density, J. Power Sources 317 (2016) 49-56. https://doi.org/10.1016/j.jpowsour.2016.03.080

[7] J. Urban, F. Svec, J. M. Fréchet, Efficient separation of small molecules using a large surface area hypercrosslinked monolithic polymer capillary column, Anal. Chem. 82 (2010) 1621-1623. https://doi.org/10.1021/ac100008n.

[8] C. Lu, S. Liu, J. Xu, Y. Ding, G. Ouyang, Exploitation of a microporous organic polymer as a stationary phase for capillary gas chromatography, Anal. Chim. Acta 902 (2016) 205-211. https://doi.org/10.1016/j.aca.2015.10.034.

[9] C. Perego, R. Millini, Porous materials in catalysis: challenges for mesoporous materials, Chem. Soc. Rev. 42 (2013) 3956- 3976. https://doi.org/10.1039/C2CS35244C

[10] H. Gao, L. Ding, W. Li, G. Ma, H. Bai, L. Li, Hyper-cross-linked organic microporous polymers based on alternating copolymerization of bismaleimide, ACS Macro Lett. 5 (2016) 377-381. https://doi.org/10.1021/acsmacrolett.6b00015.

[11] R. Castaldo, R. Avolio, M. Cocca, G. Gentile, M. E. Errico, M. Avella, V. Ambrogi, A versatile synthetic approach toward hyper-cross-linked styrene-based polymers and nanocomposites, Macromolecules 50 (2017) 4132-4143. https://doi.org/10.1021/acs.macromol.7b00812.

[12] M. Salzano de Luna, R. Castaldo, R. Altobelli, L. Gioiella, G. Filippone, G. Gentile, V. Ambrogi, Chitosan hydrogels embedding hyper-crosslinked polymer particles as reusable broad-spectrum adsorbents for dye removal, Carbohydr. Polym. 177 (2017) 347-354. http://dx.doi.org/10.1016/j.carbpol.2017.09.006.

[13] Castaldo, R., Gentile, G., Avella, M., Carfagna, C., Ambrogi, V., 2017. Microporous hyper-crosslinked polystyrenes and nanocomposites with high adsorption properties: a review. Polymers. 9, 651. http://dx.doi.org/10.3390/polym9120651.

[14] M. P. Tsyurupa, V. A. Davankov, Porous structure of hypercrosslinked polystyrene: state-of-the-art mini-review, React. Funct. Polym. 66 (2006) 768-779. https://doi.org/10.1016/j.reactfunctpolym.2005.11.004.

[15] L. Ding, H. Gao, F. Xie, W. Li, H. Bai, L. Li, Porosity-enhanced polymers from hyper-cross-linked polymer precursors, Macromolecules 50 (2017) 956-962. https://doi.org/10.1021/acs.macromol.6b02715.

[16] G. Xiao, R. Wen, A. Liu, G. He, D. Wu, Adsorption performance of salicylic acid on a novel resin with distinctive double pore structure, J. Hazard. Mater. 329 (2017) 77-83. https://doi.org/10.1016/j.jhazmat.2017.01.030.

[17] R. Castaldo, R. Avolio, M. Cocca, G. Gentile, M. E. Errico, M. Avella, V. Ambrogi. Synthesis and adsorption study of hypercrosslinked styrene-based nanocomposites containing multi-walled carbon nanotubes, RSC Adv. 7 (2017) 6865- 6874. https://doi.org/10.1039/c6ra25481k.

[18] P. A. G. Cormack, A. Davies, N. Fontanals, Synthesis and characterization of microporous polymer microspheres with strong cation-exchange character, React. Funct. Polym. 72 (2012) 939-946. https://doi.org/10.1016/j.reactfunctpolym.2012.08.003.

[19] S. Bhunia, B. Banerjee, A. Bhaumik, A new hypercrosslinked supermicroporous polymer, with scope for sulfonation, and its catalytic potential for the efficient synthesis of biodiesel at room temperature, Chem. Comm. 51 (2015) 5020-5023. https://doi.org/10.1039/C4CC09872B.

[20] M. G. Plaza, C. Pevida, A. Arenillas, F. Rubiera, CO_2 capture by adsorption with nitrogen enriched carbons, J. J. Pis. Fuel 86 (2007) 2204-2212. https://doi.org/10.1016/j.fuel.2007.06.001.

[21] P. Krajnc, J. F. Brown, N. R. Cameron, Monolithic scavenger resins by amine functionalizations of poly (4-vinylbenzyl chloride-co-divinylbenzene) PolyHIPE materials, Org. Lett. 4 (2002) 2497-2500. https://doi.org/10.1021/ol026115k.

[22] E. E. Ünveren, B. Ö. Monkul, Ş. Sarıoğlan, N. Karademir, E. Alper, Solid amine sorbents for CO_2 capture by chemical adsorption: a review, Petroleum 3 (2017) 37-50. https://doi.org/10.1016/j.petlm.2016.11.001.

[23] F. Liu, S. Wang, G. Lin, S. Chen, Development and characterization of amine-functionalized hyper-cross-linked resin for CO_2 capture, New J. Chem. 42 (2018) 420-428. https://doi.org/10.1039/C7NJ03421K.

[24] K. A. Fayemiwo, G. T. Vladisavljević, S. A. Nabavi, B. Benyahia, D. P. Hanak, K. N. Loponov, V. Manović, Nitrogen-rich hyper-crosslinked polymers for low-pressure CO_2 capture, Chem. Eng. J. 334 (2018) 2004-2013. https://doi.org/10.1016/j.cej.2017.11.106.

[25] T. Zhang, F. Zhou, J. Huang, R. Man, Ethylene glycol dimethacrylate modified hyper-cross-linked resins: Porogen effect on pore structure and adsorption performance, Chem. Eng. J. 339 (2018) 278-287. https://doi.org/10.1016/j.cej.2018.01.138.

[26] T. Zhang, J. Huang, Tunable synthesis of the polar modified hyper-cross-linked resins and application to the adsorption, J. Colloid Interface Sci. 505 (2017) 383-391. https://doi.org/10.1016/j.jcis.2017.06.030.

[27] R. Avolio, G. Gentile, M. Avella, D. Capitani, M. E. Errico, Synthesis and characterization of poly(methylmethacrylate)/silica nanocomposites: Study of the interphase by solid-state NMR and structure/properties relationships, J. Polym Sci. A Polym. Chem. 48 (2010) 5618-5629. https://doi.org/10.1002/pola.24377.

[28] M. Thommes, K. Kaneko, A. V. Neimark, J. P. Olivier, F. Rodriguez-Reinoso, J. Rouquerol, K. S. Sing, Physisorption of gases, with special reference to the evaluation of surface area and pore size distribution (IUPAC Technical Report), Pure Appl. Chem. 87 (2015) 1051-1069. https://doi.org/10.1515/pac-2014-1117.

[29] J.-H. Ahn, J.-E. Jang, C.-G. Oh, S.-K. Ihm, J. Cortés and D. C. Sherrington, Rapid generation and control of microporosity, bimodal pore size distribution, and surface area in Davankov-type hyper-cross-linked resins, Macromolecules 39 (2006) 627-632. https://doi.org/10.1021/ma051152n.

[30] S. K. Das, P. Bhanja, S. K. Kundu, S. Mondal, A. Bhaumik, Role of surface phenolic-OH groups in n-rich porous organic polymers for enhancing the CO_2 uptake and CO_2/N_2 selectivity: experimental and computational studies, ACS Appl. Mater. Interfaces 10 (2018) 23813-23824. https://doi.org/10.1021/acsami.8b05849.

[31] Xing, W., Liu, C., Zhou, Z., Zhou, J., Wang, G., Zhuo, S., Xue, Q., Song, L., Yan, Z., 2014. Oxygen-containing functional group-facilitated CO_2 capture by carbide-derived carbons. Nanoscale Res. Lett. 9, 189. https://doi.org/10.1186/1556-276X-9-189.

[32] H. Li, B. Meng, S. M. Mahurin, S.-H. Chai, K. M. Nelson, D. C. Baker, H. Liu, S. Dai, Carbohydrate based hyper-crosslinked organic polymers with –OH functional groups for CO_2 separation, J. Mater. Chem. A 3 (2015) 20913-20918. https://doi.org/10.1039/C5TA03213J.

[33] A. L. Myers, J. M. Prausnitz, Thermodynamics of mixed-gas adsorption, AIChE J. 11 (1965) 121-127. https://doi.org/10.1002/aic.690110125.

[34] T. M. McDonald, D. M. D'Alessandro, R. Krishna, J. R. Long, Enhanced carbon dioxide capture upon incorporation of N,N′-dimethylethylenediamine in the metal–organic framework CuBTTri, Chem. Sci. 2 (2011) 2022-2028. https://doi.org/10.1039/C1SC00354B.

[35] S. Gadipelli, V. Krungleviciute, G. Zheng-Xiao, Y. Taner, Exceptional CO_2 capture in a hierarchically porous carbon with simultaneous high surface area and pore volume, Energy Environ. Sci. 7 (2014) 335-342. https://doi.org/10.1039/C3EE42918K.

[36] Z. Zhang, J. Zhou, W. Xing, Q. Xue, Z. Yan, S. Zhuo, S. Z. Qiao, Critical role of small micropores in high CO_2 uptake, Phys. Chem. Chem. Phys. 15 (2013) 2523-2529. https://doi.org/10.1039/C2CP44436D.

SUPPLEMENTARY INFORMATION

Functional hyper-crosslinked resins with tailored adsorption properties for environmental applications

Rachele Castaldo[a], Veronica Ambrogi[b], Roberto Avolio[a], Mariacristina Cocca[a], Gennaro Gentile[a,*], Maria Emanuela Errico[a], Maurizio Avella[a]

[a] Institute for Polymers, Composites and Biomaterials, National Research Council of Italy, Via Campi Flegrei 34, 80078 Pozzuoli, Italy

[b] Department of Chemical, Materials and Production Engineering, University of Naples Federico II, Piazzale Tecchio 80, 80125 Napoli, Italy

*Corresponding author. E-mail address: gennaro.gentile@cnr.it

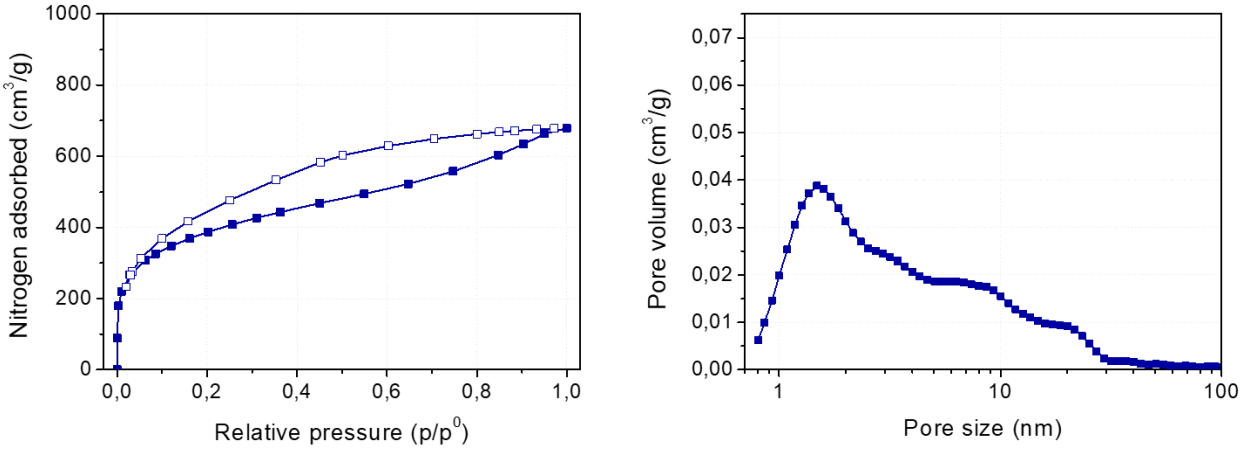

Figure S1. Nitrogen adsorption isotherm (left) and DFT pore size distribution (right) of XDV-5min.